Observations of relativistic electron precipitation due to combined scattering of whistler-mode and EMIC waves

M. Fraz Bashir [1], Anton Artemyev [1,2], Xiao-Jia Zhang [3,1], Vassilis Angelopoulos [1], E. Tsai[1], and C. Wilkins[1]

[1]Earth, Planetary, and Space Sciences, University of California, Los Angeles, Los Angeles, CA 90095, USA
[2]Space Research Institute, RAS, Moscow, Russia
[3]Department of Physics, University of Texas at Dallas, Richardson, TX, USA

Key Points:

- We report observations of energetic electron precipitation likely driven by concurrent whistle-mode and EMIC waves
- The combined scattering of whistler-mode and EMIC waves leads to electron precipitation over a wide energy range of 50 keVs to a few MeVs
- This study highlights the importance of nonlinear effects for explaining the observed energetic electron fluxes in the inner magnetosphere

Corresponding author: Muhammad Fraz Bashir, frazbashir@epss.ucla.edu

Abstract

The two most important wave modes responsible for energetic electron scattering to the Earth's ionosphere are electromagnetic ion cyclotron (EMIC) waves and whistler-mode waves. In this study, we report the direct observations of energetic electron (from 50 keV to 2.5 MeV) scattering driven by the combined effect of whistler-mode and EMIC waves using ELFIN measurements. We analyze several events exhibiting such properties, and show that electron resonant interactions with whistler-mode waves may enhance relativistic electron precipitation by EMIC waves. During a prototypical event which benefits from conjugate THEMIS measurements, we demonstrate that below the minimum resonance energy (E_{min}) of EMIC waves, the whistler-mode wave may both scatter electrons into the loss-cone and also accelerate them to higher energy (1-3 MeV). These accelerated electrons above E_{min} resonate with EMIC waves that, in turn, quickly scatter those electrons into the loss-cone. This enhances relativistic electron precipitation beyond what EMIC waves alone could achieve.

Plain Language Summary

Energetic electron precipitation into the upper atmosphere is an important loss process of the Earth's inner magnetosphere. Whistler-mode and electromagnetic ion cyclotron (EMIC) waves are the two most important wave modes responsible for energetic electron scattering to the Earth's ionosphere through wave-particle interaction. Although these wave modes typically drive electron losses of different energy ranges (above 1 MeV for EMIC waves and tens to hundreds of keV for whistler-mode waves), the loss mechanism due to the combined effects of EMIC and whistler-mode waves is not well-understood. We report the first direct observation of energetic electron scattering driven by the combined effect of whistler-mode and EMIC waves. Our results from equatorial and low-altitude observations, and from a data-driven test particle simulation explain the wide energy range of electron precipitation from tens of keVs to a few MeVs due to the combined whistler-mode and EMIC waves effect.

1 Introduction

Electromagnetic ion cyclotron (EMIC) and whistler-mode waves are the two main wave modes responsible for energetic electron scattering and precipitation from the Earth's radiation belts into the atmosphere (see reviews by Millan & Thorne, 2007; Li & Hudson, 2019; Thorne et al., 2021). EMIC waves are mostly responsible for the precipitation of relativistic (> 1MeV) electrons (e.g., Usanova et al., 2014; Blum et al., 2015; Shprits et al., 2016, 2017; Ni et al., 2015; Grach & Demekhov, 2020; Bashir & Ilie, 2018, 2021; Bashir et al., 2022b; Capannolo et al., 2018, 2022), whereas whistler-mode waves are very effective in precipitating sub-MeV electrons (see, e.g., reviews by Shprits et al., 2008; Ni et al., 2016; Artemyev et al., 2016; Thorne et al., 2021). Resonant scattering of relativistic (> 1MeV) electrons by whistler-mode waves is most effective at higher electron pitch-angles, which may not result in precipitation (e.g., Summers & Omura, 2007). However, the combined effect of EMIC and whistler-mode waves may enable a rapid decrease of relativistic electron fluxes: whistler-mode waves scatter electrons at higher pitch-angles toward the lower pitch-angle range, where resonance with EMIC waves may quickly scatter these electrons into the loss-cone (e.g., Mourenas et al., 2016; Zhang et al., 2017; Bashir et al., 2022a). Therefore, relativistic electron losses by combined EMIC and whistler-mode wave scattering may critically control the radiation belt dynamics (Drozdov et al., 2020). However, in contrast to electron resonance with EMIC waves providing only pitch-angle scattering (e.g., Summers & Thorne, 2003), resonance with whistler-mode waves can result in both pitch-angle and energy (acceleration) scattering (e.g., Summers, 2005; Glauert & Horne, 2005). If such acceleration is sufficiently fast and efficient, EMIC waves may scatter the newly formed relativistic electron population, those accelerated by whistler-

mode waves, into the loss cone (see discussion in Bashir et al., 2022a). Such precipitation may not require preexisting relativistic electron fluxes, and would not lead to the decrease of preexisting, e.g., previously stably trapped, relativistic electron fluxes. This study combines near-equatorial wave measurements and low-altitude electron precipitation measurements to provide direct evidence for this process in the radiation belts.

To provide a new population of relativistic electrons for subsequent EMIC-driven scattering, electron acceleration by whistler-mode waves should be sufficiently fast. The quasi-linear diffusion rates for average wave intensities show that pitch-angle scattering by EMIC waves is much faster than acceleration by whistler-mode waves (see, e.g., Glauert & Horne, 2005; Summers et al., 2007b). However, very intense whistler-mode waves may resonate with electrons nonlinearly and lead to the rapid formation of relativistic electrons via phase trapping into the turning acceleration (see Omura et al., 2007; Summers & Omura, 2007; Hsieh & Omura, 2017; Hsieh et al., 2020; Bashir et al., 2022a). The rate of this acceleration mechanism may approach the rate of pitch-angle diffusion by EMIC waves, and thus can potentially provide rapid electron acceleration and subsequent losses. In contrast to the simple phase trapping acceleration associated with pitch-angle increase (e.g., Bortnik et al., 2008; Vainchtein et al., 2018), turning acceleration will lead to a pitch-angle decrease with energy increase (Omura et al., 2007), i.e., accelerated particles are transported toward the loss-cone where EMIC waves will scatter them. Thus, additionally to the analysis of electron precipitation events with the combined effect of EMIC and whistler-mode waves, we will focus on a case study with equatorial observations of very intense whistler-mode waves simultaneously observed with EMIC waves.

We use equatorial wave measurements from THEMIS (Angelopoulos, 2008) and low-altitude precipitation measurements from ELFIN (Angelopoulos et al., 2020) to investigate the effect of electron resonant acceleration by whistler-mode waves and the subsequent scattering into the atmosphere by EMIC waves. Section 2 provides an overview of four ELFIN events exhibiting clear signatures of the combined operation of whistler-mode and EMIC waves, Section 3 describes in detail one event benefiting from ELFIN and THEMIS conjunction observations whereas Section 4 discusses possible mechanisms responsible for the enhanced precipitation of relativistic electrons in the simultaneous presence of EMIC and whistler-mode waves. Section 5 summarizes our main findings.

2 ELFIN Observations of Relativistic Electron Precipitation

We use data from the ELFIN-A CubeSat which is equipped with energetic electron detector measuring 50 keV to 6 MeV electrons with an energy resolution of $\Delta E/E < 40\%$ and covering the full (180°) pitch angle twice over a 3 s spin period. Because of its high energy resolution, ELFIN can distinguish precipitation events driven by whistler-mode waves or by EMIC waves (Grach et al., 2022; An et al., 2022; Tsai et al., 2022; Zhang et al., 2022; Angelopoulos et al., 2023). Thus, we focus on putative combined precipitation events which demonstrate properties of both whistler-mode and EMIC wave-driven precipitation.

Figure 1 shows four ELFIN orbits with signatures of electron precipitation due to EMIC and whistler-mode waves. The typical minimum resonance energy for EMIC waves is $\sim 0.5-1$MeV (Summers et al., 2007a; Kersten et al., 2014), so only the part of precipitation above a certain energy should be interpreted as evidence of EMIC-driven precipitation (see the detailed analysis of such events in Angelopoulos et al., 2023). Typical minimum resonance energy for whistler-mode waves (low band chorus waves) is below 10keV (Ni et al., 2012), whereas the scattering rate of electrons by whistler-mode waves decreases with increasing energy (Summers et al., 2007a). Thus, ELFIN observations of precipitation bursts with precipitating-to-trapped flux ratio maximizing at low energies should be interpreted as evidence of whistler-mode wave-driven precipitation (see the detailed analysis of such events in Tsai et al., 2022; Zhang et al., 2022). Mid-

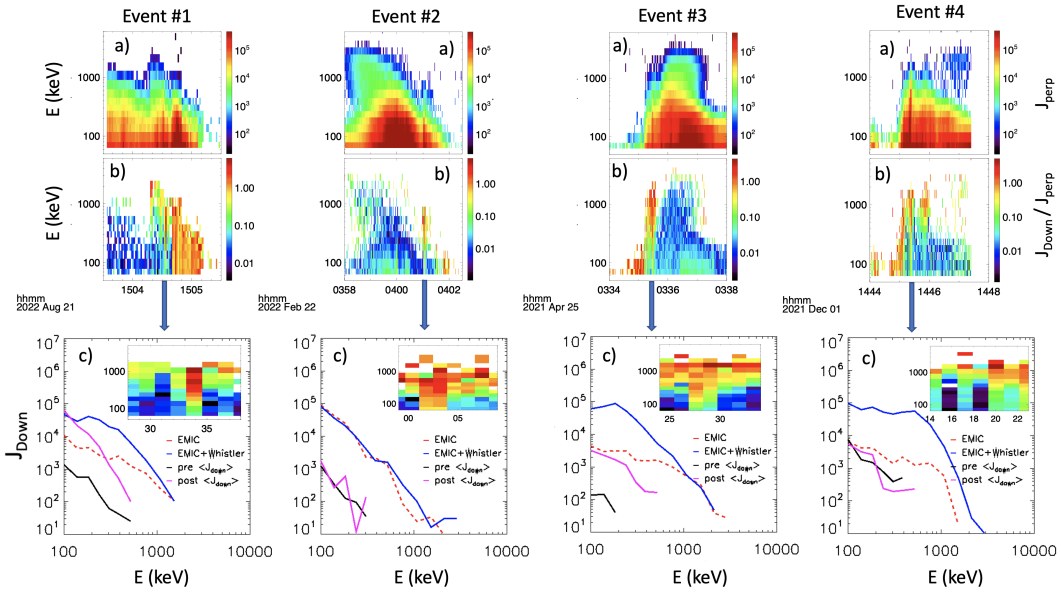

Figure 1. Four events of ELFIN observations of electron precipitation: top panels (a) show locally trapped (i.e., outside the local loss cone, or near-perpendicular) electron fluxes j_{perp}; middle panels (b) show precipitating (down-going)-to-trapped flux ratio (j_{down}/j_{perp}); bottom panels (c) show energy spectra of precipitating electrons during subintervals (shown by arrow and corresponding panel inserts) with relativistic and subrelativistic electron precipitation bursts exhibiting EMIC-only and EMIC & whistler-mode wave signatures. Bottom panels also include the average background fluxes before (pre $\langle j_{down} \rangle$) and after (post $\langle j_{down} \rangle$) each subinterval.

dle panels of Figure 1 show that precipitation events contain both spin-scale bursts with EMIC-driven precipitation only (j_{down}/j_{perp} maximizing at relativistic energies) and bursts with combined whistler-mode and EMIC effects (j_{down}/j_{perp} is high over the entire energy range). Therefore, we may interpret these events as short-time-scale whistler-driven precipitation bursts embedded within large-time-scale EMIC-driven precipitation. The scale difference is likely due to the different spatial scales of equatorial generation regions of EMIC waves (thousands of km, see Blum et al., 2016, 2017; Angelopoulos et al., 2023) and whistler-mode waves (hundreds of km, see Agapitov et al., 2017). Note that the precipitating flux levels during precipitation bursts are much higher than the background precipitating fluxes levels i.e., indeed these observations allow us to compare the efficiency of EMIC-only versus EMIC and whistler-mode burst-driven precipitation with no contribution from background waves. The bottom panels of Figure 1 demonstrate that in the presence of whistler-mode waves, not only precipitation of sub-relativistic electrons ($<$ 500keV) is enhanced, which should be directly scattered by whistler-mode waves, but precipitation of relativistic electrons (likely scattered by EMIC waves) is also enhanced.

3 Event with ELFIN/THEMIS Observations of EMIC and Whistler Waves

This section describes an event with ELFIN-A measurements similar to those shown in Figure 1, but with conjugate, near-equatorial wave measurements by THEMIS. Figure 2 shows the ELFIN-A measurements which were collected on 29 April 2021, at L-shell $\sim$ 5 near the dawn sector of the southern hemisphere. At $\sim$ 04:10:40 UT, precipitating (down-going) fluxes (J_{down}) of 300 keV to 2.5 MeV electrons suddenly increase

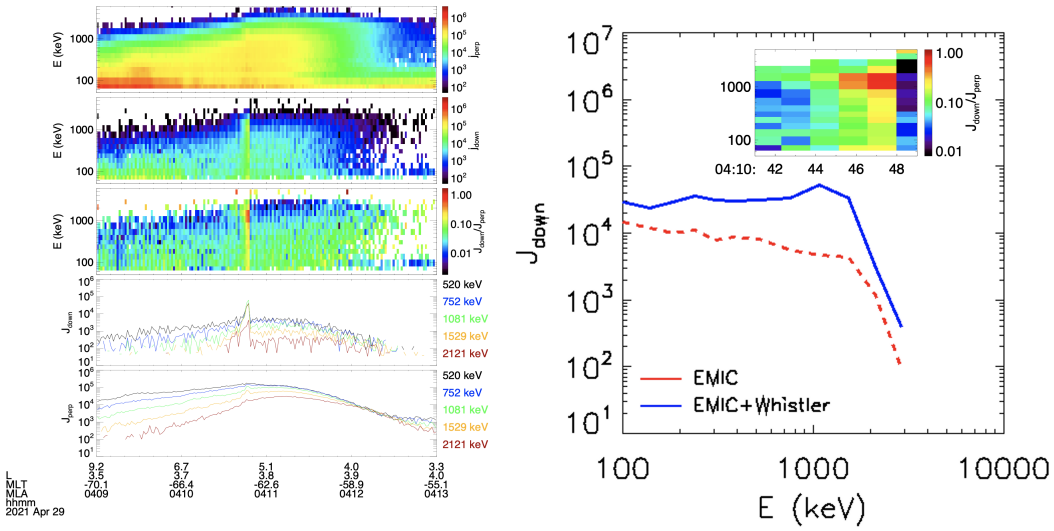

Figure 2. Overview of ELFIN-A observations (left panels): locally trapped fluxes (j_{perp}), precipitating or down-going fluxes (j_{down}), precipitating-to-trapped flux ratio (j_{down}/j_{perp}), 1D spectra j_{down} and j_{perp} at five energy channels (520 keV-2121 keV). L, MLT, and MLAT of ELFIN-A are marked at the bottom. The right panel depicts the average precipitating fluxes as a function of energy due to combined EMIC and whistler-mode waves (solid-blue curve) and EMIC waves only (dashed-red curve) for the sub-interval (as shown by down-to-perpendicular flux ratio inserted spectrogram similar to Figure 1 bottom panels)

with the highest precipitating to trapped flux ratio above 1 MeV. The locally trapped (near-perpendicular) electron fluxes (J_{perp}) show enhancement over a wide range of L-shells (4-6.5), exhibiting low precipitating to trapped flux ratio (J_{down}/J_{perp} is mostly less than 0.1) except for a few spins around 04:10:40 UT where this ratio can be greater than 0.5. The most intense burst of precipitation shows J_{down}/J_{perp} enhancement maximizing at relativistic energies $\sim$ 1MeV (the typical range of EMIC-driven precipitation), but extending down to 50keV (the typical range of whistler-wave-driven precipitation). Note that the enhanced relativistic electron precipitation lasts longer than the enhancement of $<$ 500 keV precipitation (which only lasts for a single spin). This is indicative of a short whistler-mode burst embedded within a large-scale EMIC generation region.

During this event, ELFIN magnetically mapped close to the near-equatorial THEMIS-E spacecraft (Angelopoulos, 2008), which, at the time, was moving from lower L to higher L, observed the pertinent EMIC and whistler-mode waves and measured the properties of the cold plasma, and magnetic fields. We use magnetic field data from Flux Gate Magnetometer (FGM)(Auster et al., 2008). During fast mode, FGM measures waveforms at a time resolution of 1/16 s, sufficient to resolve the EMIC wave frequency range. Measurements of the THEMIS Search Coil Magnetometer (Le Contel et al., 2008) well cover the whistler-mode frequency range. The cold plasma density is inferred from the spacecraft potential (Nishimura et al., 2013) measured by THEMIS Electric Field Instrument (Bonnell et al., 2008).

Supplementary Figure S1 shows that during this event, THEMIS-E observed whistler-mode waves around and outside of the plasmapause, identified as a strong plasma frequency (plasma density) gradient. At the plasmapause, THEMIS-E also observed He^+ band EMIC waves (field-aligned, left-hand polarized waves). The ratio of plasma to electron cyclotron frequency, $f_{pe}/f_{ce,eq}$, varies from $\sim$ 20 to 5 across the plasmapause. Note

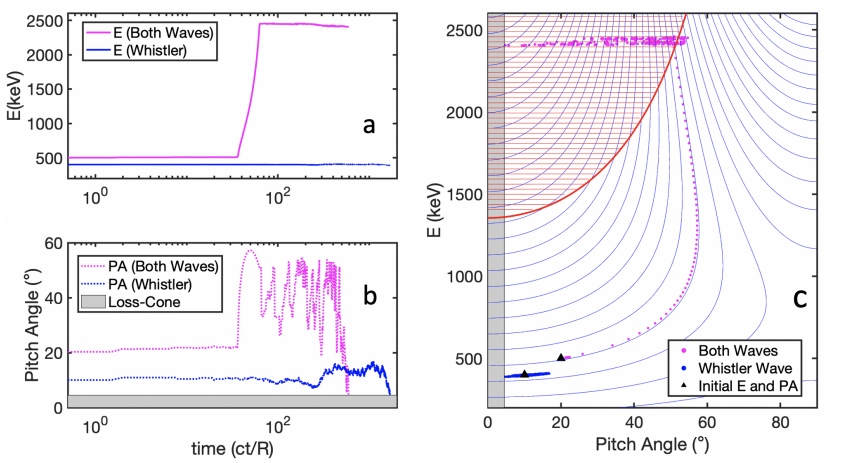

Figure 3. Illustrative electron trajectories from our simulations. Panels (a,b) depict the temporal (in units of ct/LR_E) evolution of the electron's energy and pitch angle for whistler-mode waves only (blue curve) and for the combined effect (magenta curve) of whistler-mode and EMIC waves. The loss-cone (assumed to be 4.5 °) is shaded in grey in Panel (b). Panel (c) shows the same trajectories on an energy, pitch-angle plane, with resonance curves for whistler-mode (blue curves) and EMIC (red lines) waves overlaid, and the range of EMIC resonance energies is shown by a thick red curve. The blue dots show electron trajectory (starting at an initial energy of 400keV and an equatorial pitch angle of 10 °, represented by the triangle) directly scattered by whistler waves into loss-cone; the other electron trajectory (magenta dots), with an initial energy of 500 keV and an equatorial pitch angle of 20 °, show that the electron gets accelerated by whistler waves and then quickly scattered into loss-cone by EMIC waves.

that the projection of ELFIN to the equatorial plane is subject to uncertainties of empirical magnetic field models. Thus, this THEMIS-ELFIN conjunction is only approximate. ELFIN observations of relativistic electron precipitation burst and THEMIS observations of EMIC waves are within the $\Delta L = \pm 1$, $\Delta MLT = 2$ of each other. These ranges are comparable to the spatial scale of the typical EMIC wave source region (Blum et al., 2016, 2017), whereas an $\sim$ 40min time difference between THEMIS and ELFIN observations is within the lifetime of EMIC wave source region (Engebretson et al., 2015; Blum et al., 2020). Whistler mode waves are observed by all three THEMIS probes during the entire $\sim$ 2 hour interval within the $\Delta MLT \sim 2$ domain. However, we should note that the EMIC burst is observed by THEMIS E only, whereas A and D located $\pm 1.5 R_E$ away from E do not detect these EMIC bursts. Thus, we cannot exclude the possibility of a small-scale EMIC source region (e.g., Frey et al., 2004). But ELFIN observations of relativistic electron precipitation without $\sim$ 50keV precipitation (two spins before the main precipitation burst, see the inserted panel in Fig. 2) confirm that there was scattering by equatorial EMIC waves, which may relate to THEMIS-E observations.

4 Discussion

Figures 1, 2 show that the presence of whistler-mode waves may enhance the precipitation of relativistic electrons. One possible mechanism of such enhancement is that intense whistler-mode waves drive electron acceleration (e.g., turning acceleration, see Omura et al., 2007; Summers & Omura, 2007), and the accelerated electrons supplement the population that are to be scattered by EMIC waves (Bashir et al., 2022a). In order to verify this scenario, we perform simple test particle simulations. The simulation is based

on Hamiltonian equations for a monochromatic wave (see Vainchtein et al., 2018; Artemyev et al., 2021), and this simplification (constant wave frequency) may reduce the efficiency of wave-particle resonant interactions (see discussion of frequency drift contribution in Demekhov et al., 2006; Katoh & Omura, 2007; Hiraga & Omura, 2020).

We consider the precipitation event of Figure 2, for which we have near-equatorial observations of waves (see the supplementary information). For the whistler wave, we use the frequency $f_{wh}/f_{ce,eq} = 0.3$ & 0.4, the observed wave amplitude at $B_{w,wh} = 500$ pT $\cdot\Lambda(\lambda)$, the whistler wave latitudinal profile modeled as $\Lambda(\lambda) = 0.5\cdot(1+\tanh(\lambda/\delta\lambda_1))\exp\left(-(\lambda/\delta\lambda_2)^2\right)$ and $\delta\lambda_{1,2} = 1^\circ, 40^\circ$ (e.g., we assume wave generation at the equator and damping at high latitudes, see details of this empirical wave model in Agapitov et al., 2018). For the ducted whistler case, we have used $\Lambda(\lambda) \to 1$. We also include wave field modulation by assuming whistler-mode waves propagate in wave packets: $B_{w,wh} \to B_{w,wh}\cdot\Phi(l)$ with $\Phi(l) = \exp(-0.25\cdot(\sin(\phi/(2\pi l))^2))$, where ϕ is the wave phase and $l = 300$ determines the wave-packet size (we use the longest wave packets from observations, see statistics in Zhang et al., 2019, 2021).

For the He^+ band EMIC wave, we use the most intense wave from observations, with an amplitude of $B_{w,EMIC} = 500$ pT, at a fixed frequency $f_{EMIC}/f_{cp,eq} = 0.2$. Plasma composition is assumed to be 20% helium and 80% cold protons (Lee et al., 2012; Lee & Angelopoulos, 2014), and latitudinal distribution of EMIC waves as $B_{w,EMIC} \to B_{w,EMIC}\cdot\Lambda(\lambda)$ with $\Lambda(\lambda) = 0.5(\tanh(\lambda/\delta\lambda_1) - \tanh((\lambda-\delta\lambda_2)/\delta\lambda_1))$ with $\delta\lambda_{1,2} = 1^\circ, 15^\circ$, i.e., there is no EMIC wave around and above the helium resonance latitude that is around $\sim 25^\circ$ for the selected wave frequency. For this study, we used the field-aligned cold plasma dispersion relation for both whistler and EMIC waves (Stix, 1962), with $f_{pe}/f_{ce,eq} = 20$, and $L = 4.5$. The time is normalized to a typical scale R/c$\sim$ 0.1 s as R=4.5 R_E, where R_E is the radius of the Earth and c is the speed of light and simulation in time units is run for 200 seconds (see figure S4 for more details).

Figure 3 shows two loss mechanisms of energetic electrons with+ initial pitch-angles that are not in resonance with EMIC waves: (1) electrons directly scattered into the loss-cone by whistler-mode waves (blue trajectory) or (2) electrons phase trapped and accelerated by whistler-mode waves to energies sufficiently high for resonance with EMIC waves, and then scattered into loss-cone by EMIC waves (magenta trajectory). Resonance with whistler-mode waves moves electrons along the resonance curves (Summers et al., 1998), and thus we are interested in those that will cross the region (above the E_{min} shown by thick red curve) of electron resonant interaction with EMIC waves (the latter interactions, primarily resulting in pitch-angle scattering, occur along the thin horizontal red lines). For moderate electron energies, phase trapping results in energy and pitch-angle increase (e.g., Bortnik et al., 2008; Vainchtein et al., 2018), and thus resonance curves move away from the loss-cone. However, when the electron energy reaches $\gamma > f_{ce}/f$, its pitch-angle starts to decrease during the phase trapping (so-called turning acceleration Omura et al., 2007; Bashir et al., 2022a). This effect bends the resonance curves back toward smaller pitch-angles. It thus allows the accelerated electron to escape from the trapping at an energy and pitch-angle where resonance with EMIC waves can occur. Supplementary information provides more examples of such a double resonance effect (trapping acceleration by whistler-mode waves followed by scattering into the loss-cone by EMIC waves).

The model results suggest the following scenario for the formation of the observed electron precipitation spectrum: The source size of EMIC waves is usually sufficiently large (Blum et al., 2016, 2017) to provide relativistic electron precipitation within an $\sim 1R_E$ region near the equator (Capannolo et al., 2019), which corresponds to several spins of ELFIN observations at low altitudes (see several examples of ELFIN observed EMIC-driven precipitation in, e.g., Grach et al., 2021; An et al., 2022; Angelopoulos et al., 2023). Therefore, the relativistic electron precipitation within 04:10:35-04:10:50 UT should be attributed to EMIC waves. At the beginning of this subinterval, there is no strong sub-

MeV precipitation (see j_{prec}/j_{trap} in Figure 2) which we assert is indicative of an absence of strong whistler-mode waves. We interpret the following burst of $<$ 1MeV precipitation around 04:10:45 UT as due to a whistler-mode wave burst (the short duration of the precipitation burst should be attributed to the small scale of whistler-mode wave source region near the equator, see Agapitov et al., 2017). This whistler-mode wave burst is sufficiently strong to provide electron acceleration, and thus efficiently increase $>$ 1MeV electron fluxes that are further precipitated by EMIC waves (see an increase of j_{trap} associated with j_{prec} increase in Figure 2). However, we shall caution that due to large uncertainties of ELFIN/THEMIS mapping and the time/spatial separation of precipitation events and THEMIS wave measurements, this interpretation is presently a reasonable hypothesis supported by the limited dataset examined, and needs to be confirmed by further multi-point and statistical analysis in the future. Moreover, we used a rather simplified wave model that may not describe all important details of wave-particle nonlinear resonances. Therefore, results shown in Figure 3 should be considered as an indication that the combined whistler-mode and EMIC resonant interactions with electrons may explain the enhanced relativistic electron precipitation observed in Figures 1, 2; but much more sophisticated and detailed simulations are needed to confirm this scenario and assess the overall efficiency of the proposed combined precipitation mechanism.

5 Conclusions

This letter reports the observation of relativistic electron precipitation driven by the scattering of EMIC waves with the effect of precipitation enhancement by concurrent whistler-mode waves. For five events, ELFIN observed electron precipitation at 300keV-2.5 MeV, and precipitating fluxes which were higher during subintervals containing both EMIC and whistler-driven precipitation, compared to subintervals of EMIC-driven precipitation alone. We propose the scenario of electron acceleration (via the nonlinear resonant acceleration, e.g., phase trapping and turning acceleration) by whistler-mode waves up to relativistic energies and subsequent scattering of this accelerated electron population by EMIC waves. Simplified test particle simulations confirm that this scenario indeed can work. Our results suggest that nonlinear resonant acceleration (Omura et al., 2007, 2015) may significantly contribute to electron precipitation events observed at low altitudes.

Acknowledgments

A.V.A, X.-J.Z., and M.F.B. acknowledge support from the NASA grants 80NSSC20K1270, 80NSSC23K0403. X.-J. Z. acknowledges support from the NSF grant 2021749. V.A. acknowledges support by NSF grants AGS-1242918, and AGS-2019950.

We are grateful to NASA's CubeSat Launch Initiative for ELFIN's successful launch in the desired orbits. We acknowledge the early support of the ELFIN project by the AFOSR, under its University Nanosat Program, UNP-8 project, contract FA9453-12-D-0285, and by the California Space Grant program. We acknowledge the critical contributions of numerous volunteer ELFIN team student members.

We also acknowledge NASA contract NAS5-02099 for use of data from the THEMIS mission. We thank K. H. Glassmeier, U. Auster, and W. Baumjohann for the use of FGM data provided under the lead of the Technical University of Braunschweig and with financial support through the German Ministry for Economy and Technology and the German Aerospace Center (DLR) under contract 50 OC 0302.

Open Research

Fluxes measured by ELFIN are available in ELFIN data archive https://data.elfin.ucla.edu/ in CDF format.

THEMIS data is available at `http://themis.ssl.berkeley.edu/data/themis`. Data analysis was done using SPEDAS V4.1 (Angelopoulos et al., 2019). The software can be downloaded from http://spedas.org/wiki/index.php?title=Downloads_and_Installation

References

Agapitov, O. V., Blum, L. W., Mozer, F. S., Bonnell, J. W., & Wygant, J. (2017, March). Chorus whistler wave source scales as determined from multipoint Van Allen Probe measurements. *Geophys. Res. Lett.*, *44*, 2634-2642. doi: 10.1002/2017GL072701

Agapitov, O. V., Mourenas, D., Artemyev, A. V., Mozer, F. S., Hospodarsky, G., Bonnell, J., & Krasnoselskikh, V. (2018, January). Synthetic Empirical Chorus Wave Model From Combined Van Allen Probes and Cluster Statistics. *Journal of Geophysical Research (Space Physics)*, *123*(1), 297-314. doi: 10.1002/2017JA024843

An, X., Artemyev, A., Angelopoulos, V., Zhang, X., Mourenas, D., & Bortnik, J. (2022, September). Nonresonant Scattering of Relativistic Electrons by Electromagnetic Ion Cyclotron Waves in Earth's Radiation Belts. *Phys. Rev. Lett.*, *129*(13), 135101. doi: 10.1103/PhysRevLett.129.135101

Angelopoulos, V. (2008, December). The THEMIS Mission. *Space Sci. Rev.*, *141*, 5-34. doi: 10.1007/s11214-008-9336-1

Angelopoulos, V., Cruce, P., Drozdov, A., Grimes, E. W., Hatzigeorgiu, N., King, D. A., ... Schroeder, P. (2019, January). The Space Physics Environment Data Analysis System (SPEDAS). *Space Sci. Rev.*, *215*, 9. doi: 10.1007/s11214-018-0576-4

Angelopoulos, V., Tsai, E., Bingley, L., Shaffer, C., Turner, D. L., Runov, A., ... Zhang, G. Y. (2020, July). The ELFIN Mission. *Space Sci. Rev.*, *216*(5), 103. doi: 10.1007/s11214-020-00721-7

Angelopoulos, V., Zhang, X. J., Artemyev, A. V., Mourenas, D., Tsai, E., Wilkins, C., ... Zarifian, A. (2023). Energetic electron precipitation driven by electromagnetic ion cyclotron waves from elfin's low altitude perspective. *Space Sci Rev*, *219*, 37. doi: https://doi.org/10.1007/s11214-023-00984-w

Artemyev, A. V., Agapitov, O., Mourenas, D., Krasnoselskikh, V., Shastun, V., & Mozer, F. (2016, April). Oblique Whistler-Mode Waves in the Earth's Inner Magnetosphere: Energy Distribution, Origins, and Role in Radiation Belt Dynamics. *Space Sci. Rev.*, *200*(1-4), 261-355. doi: 10.1007/s11214-016-0252-5

Artemyev, A. V., Neishtadt, A. I., Vasiliev, A. A., Zhang, X.-J., Mourenas, D., & Vainchtein, D. (2021, March). Long-term dynamics driven by resonant wave-particle interactions: from Hamiltonian resonance theory to phase space mapping. *Journal of Plasma Physics*, *87*(2), 835870201. doi: 10.1017/S0022377821000246

Auster, H. U., Glassmeier, K. H., Magnes, W., Aydogar, O., Baumjohann, W., Constantinescu, D., ... Wiedemann, M. (2008, December). The THEMIS Fluxgate Magnetometer. *Space Sci. Rev.*, *141*, 235-264. doi: 10.1007/s11214-008-9365-9

Bashir, M. F., Artemyev, A., Zhang, X.-J., & Angelopoulos, V. (2022a). Energetic electron precipitation driven by the combined effect of ulf, emic, and whistler waves. *Journal of Geophysical Research: Space Physics*, *127*(1), e2021JA029871. doi: https://doi.org/10.1029/2021JA029871

Bashir, M. F., Artemyev, A., Zhang, X.-J., & Angelopoulos, V. (2022b). Hot plasma effects on electron resonant scattering by electromagnetic ion cyclotron waves. *Geophysical Research Letters*, *49*(11), e2022GL099229. Retrieved from `https://agupubs.onlinelibrary.wiley.com/doi/abs/10.1029/2022GL099229` doi: https://doi.org/10.1029/2022GL099229

Bashir, M. F., & Ilie, R. (2018). A new n+ band of electromagnetic ion cyclotron

waves in multi-ion cold plasmas. *Geophysical Research Letters*, *45*(19), 10,150-10,159. Retrieved from `https://agupubs.onlinelibrary.wiley.com/doi/abs/10.1029/2018GL080280` doi: https://doi.org/10.1029/2018GL080280

Bashir, M. F., & Ilie, R. (2021). The first observation of n^+ electromagnetic ion cyclotron waves. *Journal of Geophysical Research: Space Physics*, *126*(3), e2020JA028716. doi: https://doi.org/10.1029/2020JA028716

Blum, L. W., Agapitov, O., Bonnell, J. W., Kletzing, C., & Wygant, J. (2016, May). EMIC wave spatial and coherence scales as determined from multipoint Van Allen Probe measurements. *Geophys. Res. Lett.*, *43*, 4799-4807. doi: 10.1002/2016GL068799

Blum, L. W., Bonnell, J. W., Agapitov, O., Paulson, K., & Kletzing, C. (2017, February). EMIC wave scale size in the inner magnetosphere: Observations from the dual Van Allen Probes. *Geophys. Res. Lett.*, *44*, 1227-1233. doi: 10.1002/2016GL072316

Blum, L. W., Halford, A., Millan, R., Bonnell, J. W., Goldstein, J., Usanova, M., ... Li, X. (2015, July). Observations of coincident EMIC wave activity and duskside energetic electron precipitation on 18-19 January 2013. *Geophys. Res. Lett.*, *42*, 5727-5735. doi: 10.1002/2015GL065245

Blum, L. W., Remya, B., Denton, M. H., & Schiller, Q. (2020, March). Persistent EMIC Wave Activity Across the Nightside Inner Magnetosphere. *Geophys. Res. Lett.*, *47*(6), e87009. doi: 10.1029/2020GL087009

Bonnell, J. W., Mozer, F. S., Delory, G. T., Hull, A. J., Ergun, R. E., Cully, C. M., ... Harvey, P. R. (2008, December). The Electric Field Instrument (EFI) for THEMIS. *Space Sci. Rev.*, *141*, 303-341. doi: 10.1007/s11214-008-9469-2

Bortnik, J., Thorne, R. M., & Inan, U. S. (2008, November). Nonlinear interaction of energetic electrons with large amplitude chorus. *Geophys. Res. Lett.*, *35*, 21102. doi: 10.1029/2008GL035500

Capannolo, L., Li, W., Ma, Q., Shen, X. C., Zhang, X. J., Redmon, R. J., ... Raita, T. (2019, Apr). Energetic Electron Precipitation: Multievent Analysis of Its Spatial Extent During EMIC Wave Activity. *Journal of Geophysical Research (Space Physics)*, *124*(4), 2466-2483. doi: 10.1029/2018JA026291

Capannolo, L., Li, W., Ma, Q., Zhang, X.-J., Redmon, R. J., Rodriguez, J. V., ... Reeves, G. D. (2018, July). Understanding the Driver of Energetic Electron Precipitation Using Coordinated Multisatellite Measurements. *Geophys. Res. Lett.*, *45*, 6755-6765. doi: 10.1029/2018GL078604

Capannolo, L., Li, W., Millan, R., Smith, D., Sivadas, N., Sample, J., & Shekhar, S. (2022). Relativistic electron precipitation near midnight: Drivers, distribution, and properties. *Journal of Geophysical Research (Space Physics)*, *127*, e2021JA030111. doi: 10.1029/2021JA030111

Demekhov, A. G., Trakhtengerts, V. Y., Rycroft, M. J., & Nunn, D. (2006, December). Electron acceleration in the magnetosphere by whistler-mode waves of varying frequency. *Geomagnetism and Aeronomy*, *46*, 711-716. doi: 10.1134/S0016793206060053

Drozdov, A. Y., Usanova, M. E., Hudson, M. K., Allison, H. J., & Shprits, Y. Y. (2020, September). The Role of Hiss, Chorus, and EMIC Waves in the Modeling of the Dynamics of the Multi-MeV Radiation Belt Electrons. *Journal of Geophysical Research (Space Physics)*, *125*(9), e28282. doi: 10.1029/2020JA028282

Engebretson, M. J., Posch, J. L., Wygant, J. R., Kletzing, C. A., Lessard, M. R., Huang, C.-L., ... Shiokawa, K. (2015, July). Van Allen probes, NOAA, GOES, and ground observations of an intense EMIC wave event extending over 12 h in magnetic local time. *J. Geophys. Res.*, *120*, 5465-5488. doi: 10.1002/2015JA021227

Frey, H. U., Haerendel, G., Mende, S. B., Forrester, W. T., Immel, T. J., & ØStgaard, N. (2004, October). Subauroral morning proton spots (SAMPS)

as a result of plasmapause-ring-current interaction. *Journal of Geophysical Research (Space Physics)*, *109*(A10), A10305. doi: 10.1029/2004JA010516

Glauert, S. A., & Horne, R. B. (2005, April). Calculation of pitch angle and energy diffusion coefficients with the PADIE code. *J. Geophys. Res.*, *110*, 4206. doi: 10.1029/2004JA010851

Grach, V. S., Artemyev, A. V., Demekhov, A. G., Zhang, X.-J., Bortnik, J., Angelopoulos, V., ... Roberts, O. W. (2022, September). Relativistic Electron Precipitation by EMIC Waves: Importance of Nonlinear Resonant Effects. *Geophys. Res. Lett.*, *49*(17), e99994. doi: 10.1029/2022GL099994

Grach, V. S., & Demekhov, A. G. (2020, February). Precipitation of Relativistic Electrons Under Resonant Interaction With Electromagnetic Ion Cyclotron Wave Packets. *Journal of Geophysical Research (Space Physics)*, *125*(2), e27358. doi: 10.1029/2019JA027358

Grach, V. S., Demekhov, A. G., & Larchenko, A. V. (2021, December). Resonant interaction of relativistic electrons with realistic electromagnetic ion-cyclotron wave packets. *Earth, Planets and Space*, *73*(1), 129. doi: 10.1186/s40623-021-01453-w

Hiraga, R., & Omura, Y. (2020, February). Acceleration mechanism of radiation belt electrons through interaction with multi-subpacket chorus waves. *Earth, Planets, and Space*, *72*(1), 21. doi: 10.1186/s40623-020-1134-3

Hsieh, Y.-K., Kubota, Y., & Omura, Y. (2020). Nonlinear evolution of radiation belt electron fluxes interacting with oblique whistler mode chorus emissions. *Journal of Geophysical Research: Space Physics*, e2019JA027465. Retrieved from `https://agupubs.onlinelibrary.wiley.com/doi/abs/10.1029/2019JA027465` (e2019JA027465 2019JA027465) doi: 10.1029/2019JA027465

Hsieh, Y.-K., & Omura, Y. (2017, January). Nonlinear dynamics of electrons interacting with oblique whistler mode chorus in the magnetosphere. *J. Geophys. Res.*, *122*, 675-694. doi: 10.1002/2016JA023255

Katoh, Y., & Omura, Y. (2007, July). Relativistic particle acceleration in the process of whistler-mode chorus wave generation. *Geophys. Res. Lett.*, *34*, L13102. doi: 10.1029/2007GL029758

Kersten, T., Horne, R. B., Glauert, S. A., Meredith, N. P., Fraser, B. J., & Grew, R. S. (2014, November). Electron losses from the radiation belts caused by EMIC waves. *J. Geophys. Res.*, *119*, 8820-8837. doi: 10.1002/2014JA020366

Le Contel, O., Roux, A., Robert, P., Coillot, C., Bouabdellah, A., de La Porte, B., ... Larson, D. (2008, December). First Results of the THEMIS Search Coil Magnetometers. *Space Sci. Rev.*, *141*, 509-534. doi: 10.1007/s11214-008-9371-y

Lee, J. H., & Angelopoulos, V. (2014, Mar). On the presence and properties of cold ions near Earth's equatorial magnetosphere. *Journal of Geophysical Research (Space Physics)*, *119*(3), 1749-1770. doi: 10.1002/2013JA019305

Lee, J. H., Chen, L., Angelopoulos, V., & Thorne, R. M. (2012, Jun). THEMIS observations and modeling of multiple ion species and EMIC waves: Implications for a vanishing He^+ stop band. *Journal of Geophysical Research (Space Physics)*, *117*(A6), A06204. doi: 10.1029/2012JA017539

Li, W., & Hudson, M. K. (2019, Nov). Earth's Van Allen Radiation Belts: From Discovery to the Van Allen Probes Era. *Journal of Geophysical Research (Space Physics)*, *124*(11), 8319-8351. doi: 10.1029/2018JA025940

Millan, R. M., & Thorne, R. M. (2007, March). Review of radiation belt relativistic electron losses. *Journal of Atmospheric and Solar-Terrestrial Physics*, *69*, 362-377. doi: 10.1016/j.jastp.2006.06.019

Mourenas, D., Artemyev, A. V., Ma, Q., Agapitov, O. V., & Li, W. (2016, May). Fast dropouts of multi-MeV electrons due to combined effects of EMIC and whistler mode waves. *Geophys. Res. Lett.*, *43*(9), 4155-4163. doi: 10.1002/2016GL068921

Ni, B., Cao, X., Zou, Z., Zhou, C., Gu, X., Bortnik, J., ... Xie, L. (2015, September). Resonant scattering of outer zone relativistic electrons by multiband EMIC waves and resultant electron loss time scales. *J. Geophys. Res.*, *120*, 7357-7373. doi: 10.1002/2015JA021466

Ni, B., Thorne, R. M., & Ma, Q. (2012, April). Bounce-averaged Fokker-Planck diffusion equation in non-dipolar magnetic fields with applications to the Dungey magnetosphere. *Annales Geophysicae*, *30*, 733-750. doi: 10.5194/angeo-30-733-2012

Ni, B., Thorne, R. M., Zhang, X., Bortnik, J., Pu, Z., Xie, L., ... Gu, X. (2016, April). Origins of the Earth's Diffuse Auroral Precipitation. *Space Sci. Rev.*, *200*, 205-259. doi: 10.1007/s11214-016-0234-7

Nishimura, Y., Bortnik, J., Li, W., Thorne, R. M., Ni, B., Lyons, L. R., ... Auster, U. (2013, Feb). Structures of dayside whistler-mode waves deduced from conjugate diffuse aurora. *Journal of Geophysical Research (Space Physics)*, *118*(2), 664-673. doi: 10.1029/2012JA018242

Omura, Y., Furuya, N., & Summers, D. (2007, June). Relativistic turning acceleration of resonant electrons by coherent whistler mode waves in a dipole magnetic field. *J. Geophys. Res.*, *112*, 6236. doi: 10.1029/2006JA012243

Omura, Y., Miyashita, Y., Yoshikawa, M., Summers, D., Hikishima, M., Ebihara, Y., & Kubota, Y. (2015, November). Formation process of relativistic electron flux through interaction with chorus emissions in the Earth's inner magnetosphere. *J. Geophys. Res.*, *120*, 9545-9562. doi: 10.1002/2015JA021563

Shprits, Y. Y., Drozdov, A. Y., Spasojevic, M., Kellerman, A. C., Usanova, M. E., Engebretson, M. J., ... Aseev, N. A. (2016, September). Wave-induced loss of ultra-relativistic electrons in the Van Allen radiation belts. *Nature Communications*, *7*, 12883. doi: 10.1038/ncomms12883

Shprits, Y. Y., Kellerman, A., Aseev, N., Drozdov, A. Y., & Michaelis, I. (2017, Feb). Multi-MeV electron loss in the heart of the radiation belts. *Geophys. Res. Lett.*, *44*(3), 1204-1209. doi: 10.1002/2016GL072258

Shprits, Y. Y., Subbotin, D. A., Meredith, N. P., & Elkington, S. R. (2008, November). Review of modeling of losses and sources of relativistic electrons in the outer radiation belt II: Local acceleration and loss. *Journal of Atmospheric and Solar-Terrestrial Physics*, *70*, 1694-1713. doi: 10.1016/j.jastp.2008.06.014

Stix, T. H. (1962). *The Theory of Plasma Waves*.

Summers, D. (2005, August). Quasi-linear diffusion coefficients for field-aligned electromagnetic waves with applications to the magnetosphere. *J. Geophys. Res.*, *110*, 8213. doi: 10.1029/2005JA011159

Summers, D., Ni, B., & Meredith, N. P. (2007a, April). Timescales for radiation belt electron acceleration and loss due to resonant wave-particle interactions: 1. Theory. *J. Geophys. Res.*, *112*, 4206. doi: 10.1029/2006JA011801

Summers, D., Ni, B., & Meredith, N. P. (2007b, April). Timescales for radiation belt electron acceleration and loss due to resonant wave-particle interactions: 2. Evaluation for VLF chorus, ELF hiss, and electromagnetic ion cyclotron waves. *J. Geophys. Res.*, *112*, 4207. doi: 10.1029/2006JA011993

Summers, D., & Omura, Y. (2007, December). Ultra-relativistic acceleration of electrons in planetary magnetospheres. *Geophys. Res. Lett.*, *34*, 24205. doi: 10.1029/2007GL032226

Summers, D., & Thorne, R. M. (2003, April). Relativistic electron pitch-angle scattering by electromagnetic ion cyclotron waves during geomagnetic storms. *J. Geophys. Res.*, *108*, 1143. doi: 10.1029/2002JA009489

Summers, D., Thorne, R. M., & Xiao, F. (1998, September). Relativistic theory of wave-particle resonant diffusion with application to electron acceleration in the magnetosphere. *J. Geophys. Res.*, *103*, 20487-20500. doi: 10.1029/98JA01740

Thorne, R. M., Bortnik, J., Li, W., & Ma, Q. (2021). Wave–particle interactions

in the earth's magnetosphere. In *Magnetospheres in the solar system* (p. 93-108). American Geophysical Union (AGU). doi: https://doi.org/10.1002/9781119815624.ch6

Tsai, E., Artemyev, A., Zhang, X.-J., & Angelopoulos, V. (2022, May). Relativistic Electron Precipitation Driven by Nonlinear Resonance With Whistler-Mode Waves. *Journal of Geophysical Research (Space Physics)*, *127*(5), e30338. doi: 10.1029/2022JA030338

Usanova, M. E., Drozdov, A., Orlova, K., Mann, I. R., Shprits, Y., Robertson, M. T., ... Wygant, J. (2014, March). Effect of EMIC waves on relativistic and ultrarelativistic electron populations: Ground-based and Van Allen Probes observations. *Geophys. Res. Lett.*, *41*, 1375-1381. doi: 10.1002/2013GL059024

Vainchtein, D., Zhang, X. J., Artemyev, A. V., Mourenas, D., Angelopoulos, V., & Thorne, R. M. (2018, October). Evolution of Electron Distribution Driven by Nonlinear Resonances With Intense Field-Aligned Chorus Waves. *Journal of Geophysical Research (Space Physics)*, *123*(10), 8149-8169. doi: 10.1029/2018JA025654

Zhang, X.-J., Angelopoulos, V., Mourenas, D., Artemyev, A., Tsai, E., & Wilkins, C. (2022, May). Characteristics of Electron Microburst Precipitation Based on High-Resolution ELFIN Measurements. *Journal of Geophysical Research (Space Physics)*, *127*(5), e30509. doi: 10.1029/2022JA030509

Zhang, X. J., Demekhov, A. G., Katoh, Y., Nunn, D., Tao, X., Mourenas, D., ... Angelopoulos, V. (2021, August). Fine Structure of Chorus Wave Packets: Comparison Between Observations and Wave Generation Models. *Journal of Geophysical Research (Space Physics)*, *126*(8), e29330. doi: 10.1029/2021JA029330

Zhang, X. J., Mourenas, D., Artemyev, A. V., Angelopoulos, V., Bortnik, J., Thorne, R. M., ... Hospodarsky, G. B. (2019, July). Nonlinear Electron Interaction With Intense Chorus Waves: Statistics of Occurrence Rates. *Geophys. Res. Lett.*, *46*(13), 7182-7190. doi: 10.1029/2019GL083833

Zhang, X.-J., Mourenas, D., Artemyev, A. V., Angelopoulos, V., & Thorne, R. M. (2017, August). Contemporaneous EMIC and whistler mode waves: Observations and consequences for MeV electron loss. *Geophys. Res. Lett.*, *44*, 8113-8121. doi: 10.1002/2017GL073886

Figure 1.

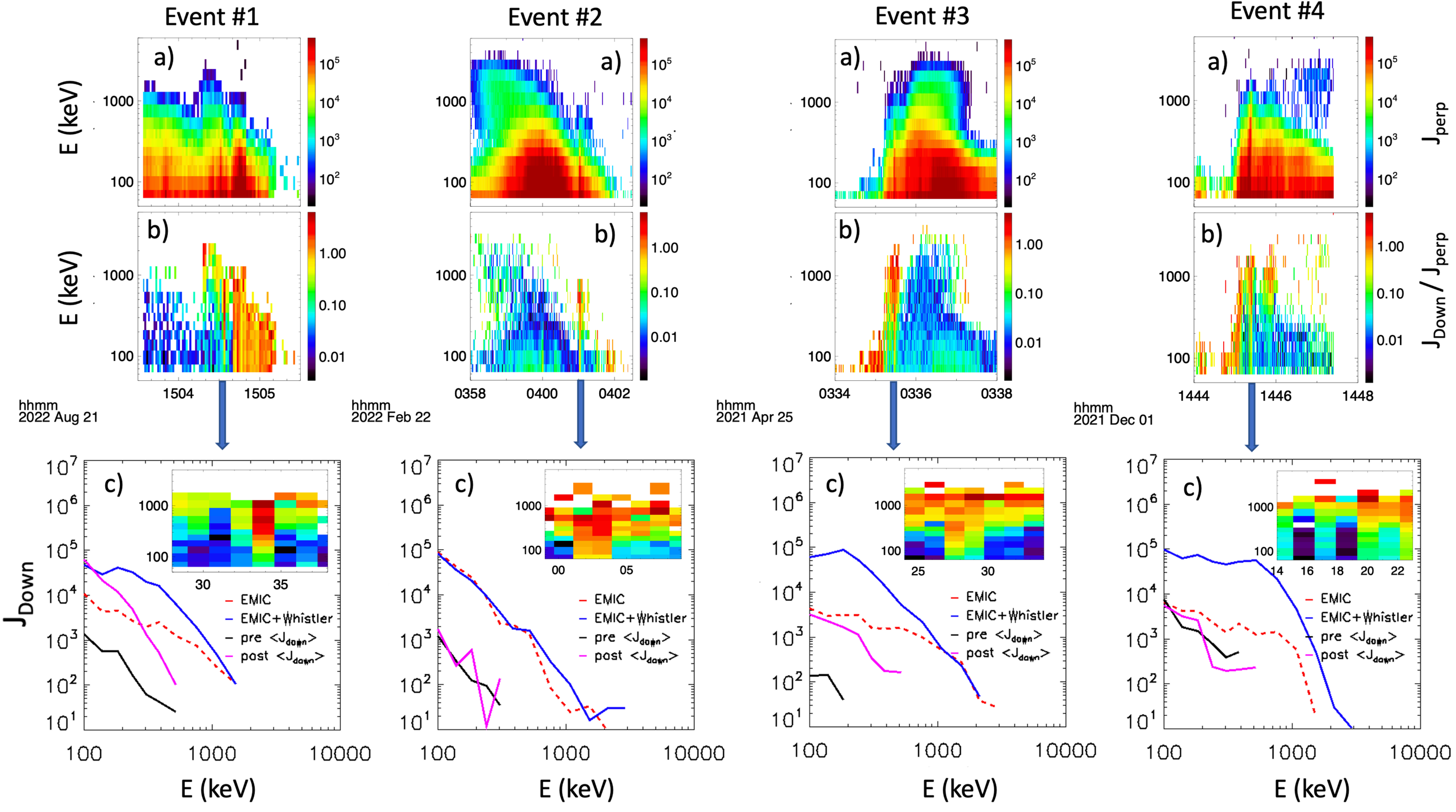
Event #1
Event #2
Event #3
Event #4
a)
b)
c)
E (keV)
1000
100
10^5
10^4
10^3
10^2
1.00
0.10
0.01
J_{perp}
J_{Down} / J_{perp}
1504
1505
0358
0400
0402
0334
0336
0338
1444
1446
1448
hhmm
2022 Aug 21
hhmm
2022 Feb 22
hhmm
2021 Apr 25
hhmm
2021 Dec 01
J_{Down}
10^7
10^6
10^5
10^4
10^3
10^2
10^1
30
35
00
05
25
30
14
16
18
20
22
EMIC
EMIC+Whistler
pre <J_{down}>
post <J_{down}>
100
1000
10000
E (keV)

Figure 2.

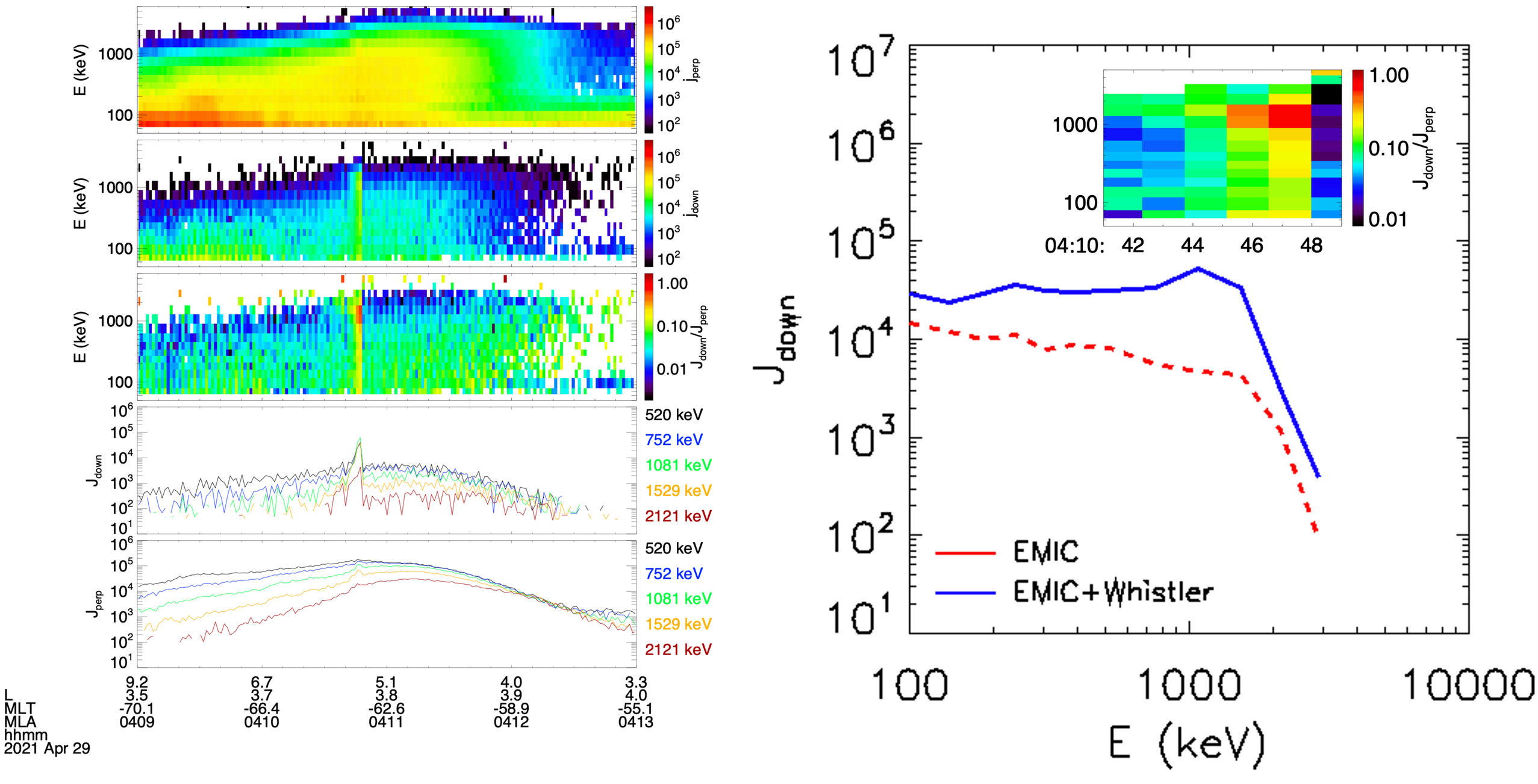
E (keV)
1000
100
j_{perp}
j_{down}
J_{down}/J_{perp}
1.00
0.10
0.01
J_{down}
J_{perp}
520 keV
752 keV
1081 keV
1529 keV
2121 keV
L
MLT
MLA
hhmm
2021 Apr 29
9.2
3.5
-70.1
0409
6.7
3.7
-66.4
0410
5.1
3.8
-62.6
0411
4.0
3.9
-58.9
0412
3.3
4.0
-55.1
0413
04:10:
42
44
46
48
EMIC
EMIC+Whistler
E (keV)
100
1000
10000

Figure 3.

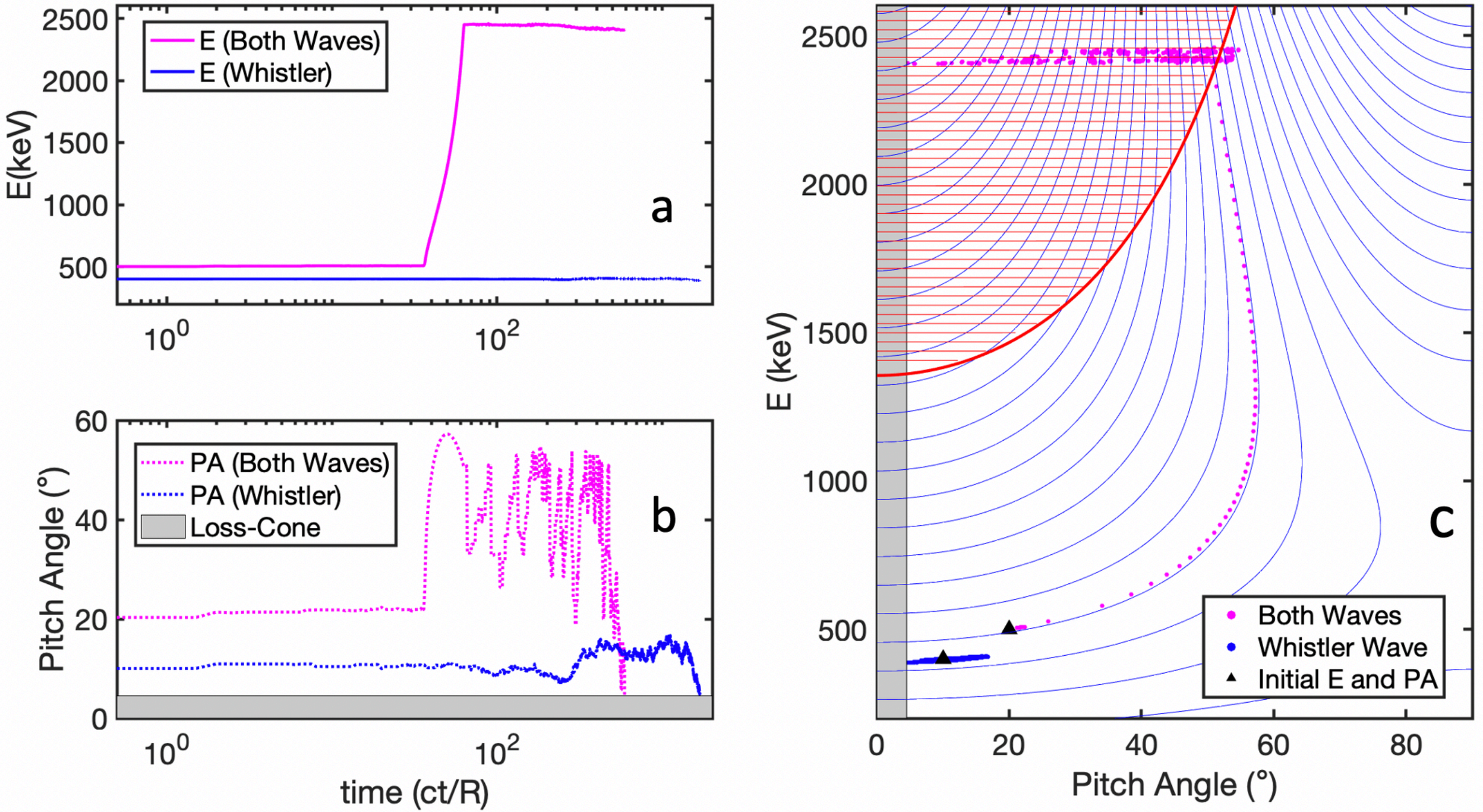
E (Both Waves)
E (Whistler)
E(keV)
2500
2000
1500
1000
500
10^0
10^2
a
PA (Both Waves)
PA (Whistler)
Loss-Cone
Pitch Angle (°)
60
40
20
0
b
time (ct/R)
E (keV)
Both Waves
Whistler Wave
Initial E and PA
0
20
40
60
80
Pitch Angle (°)
c